Proceedings of the Institution of Mechanical Engineers, Part J: Journal of Engineering Tribology
Volume 237, Issue 5, May 2023, Pages 1264-1271

https://doi.org/10.1177/13506501221132897

Special Issue: Hommage to Prof. Duncan Dowson

In vitro models of soft tissue damage by implant-associated frictional shear stresses

Jonah M. Rosas[1], Dixon J. Atkins[1], Allison L. Chau[2], Yen-Tsung Chen[3], Rachel Bae[4], Megan K. Cavanaugh[3], Ricardo I. Espinosa Lima[5], Andrew Bordeos[6], Michael G. Bryant[7], and Angela A. Pitenis[2]

Abstract

Silicone elastomer medical implants are ubiquitous in medicine, particularly for breast augmentation. However, when these devices are placed within the body, disruption of the natural biological interfaces occurs, which significantly changes the native energy-dissipation mechanisms of living systems. These new interfaces can introduce non-physiological contact pressures and tribological conditions that provoke inflammation and soft tissue damage. Despite their significance, the biotribological properties of implant-tissue and implant-extracellular matrix (ECM) interfaces remain poorly understood. Here, we developed an *in vitro* model of soft tissue damage using a custom-built *in situ* biotribometer mounted onto a confocal microscope. Sections of commercially-available silicone breast implants with distinct and clinically relevant surface roughness ($\mathbf{R_a} = 0.2 \pm 0.03\,\mu$m, $2.7 \pm 0.6\,\mu$m, and $32 \pm 7.0\,\mu$m) were mounted to spherically-capped hydrogel probes and slid against collagen-coated hydrogel surfaces as well as healthy breast epithelial (MCF10A) cell monolayers to model implant-ECM and implant-tissue interfaces. In contrast to the "smooth" silicone implants ($\mathbf{R_a} < 10\,\mu$m), we demonstrate that the "microtextured" silicone implant ($10 < \mathbf{R_a} < 50\,\mu$m) induced higher frictional shear stress ($\tau > 100$ Pa), which led to greater collagen removal and cell rupture/delamination. Our studies may provide insights into post-implantation tribological interactions between silicone breast implants and soft tissues.

Keywords

biotribology, capsular contracture, silicone breast implants, surface roughness, wound healing, fibrosis

[1]Department of Biomolecular Science and Engineering
[2]Materials Department
[3]Department of Chemical Engineering
[4]Department of Chemistry and Biochemistry
[5]College of Creative Studies, University of California, Santa Barbara, California, United States
[6]Surface Analysis Team, Keyence Microscopes, Keyence Corporation of America, El Segundo, California, United States
[7]School of Mechanical Engineering, University of Leeds, Leeds, United Kingdom

Corresponding author(s):
Angela A. Pitenis, Materials Department, University of California, Santa Barbara, Santa Barbara, California, United States 93106.
Email: apitenis@ucsb.edu

Introduction

Silicone elastomers are used in a panoply of implantable medical devices (e.g., shunts, ports, drains, biosensors, and prostheses) to adjust form and restore function. Their widespread use is partly due to their material and mechanical properties (e.g., low surface tension, thermal and chemical stability, and tunable elastic modulus) but also due to their perceived "biocompatibility."[1] These implantable materials, widely considered "inert," may provoke the foreign body response (FBR) and lead to clinical complications; certain silicone devices have been linked with chronic inflammation,[2] capsular contracture,[3] and even cancers.[4–7] Unsurprisingly, biocompatibility is a system property; there is no such thing as a universally "biocompatible material."[8] Intrinsically biocompatible systems enable materials to perform with appropriate host responses in specific situations.[9,10] It is difficult, if not impossible, to predict *in vivo* device performance without fundamental knowledge of tribological challenges across device-tissue interfaces. A wide gap in the knowledge remains regarding the delicate balance between normal and adverse cellular remodeling near implanted devices and the possible role of mechanical stresses in mediating healthy wound healing or peri-implant fibrosis. This knowledge gap is partly responsible for the lack of regulations involving surface texturing of soft breast implants. One notable case involved aggressively roughened or "macrotextured" designs (average surface roughness $\mathbf{R_a} > 50\,\mu$m), which remained on the market for decades before their voluntary recall due to a link with a rare lymphoma.[11–13] International regulatory organizations have expanded medical device testing standards to include cytotoxicity and hemocompatibility.[14] However, there are currently no recommendations nor validated pre-clinical models to assess biological responses to implant-associated tribological interactions and predict device-specific foreign body responses.

The foreign body response (FBR) initiated post-implantation begins similarly to physiological wound healing.[15,16] The FBR is characterized by a series of overlapping stages, including initial adsorption of proteins and formation of a provisional extracellular matrix (ECM), acute inflammation, and immune cell invasion associated with chronic inflammation (Figure 1).[17] The ECM provides structural support to surrounding cells as a three-dimensional network of proteins, primarily composed of collagens. Under inflamed conditions, this collagen-rich scaffold becomes a contributor to advancing fibrosis. Additionally, implant fibrosis and chronic macrophage activation and foreign body giant cell (FBGC) formation are abnormal wound-healing stages of the FBR observed post-implantation.[18] While contact with implant surfaces has been shown to directly cause the FBR, mechanical overloading and wear complications can result in implant failures and further damage, including loss of anchorage,[19] biofilm development,[20,21] and a variety of rare complications.[22] Recent advances in tribological instrumentation have enabled friction and rheological measurements between soft implant materials and living cells,[23] cell layers,[24,25] and tissues.[26] Our study investigates the relationship between silicone elastomer breast implants of varying surface roughness and damage to soft tissue models *in vitro* using collagen-coated hydrogels and cell monolayers. We hypothesize that increasing surface roughness will increase frictional shear stresses and damage soft tissues *in vitro*.

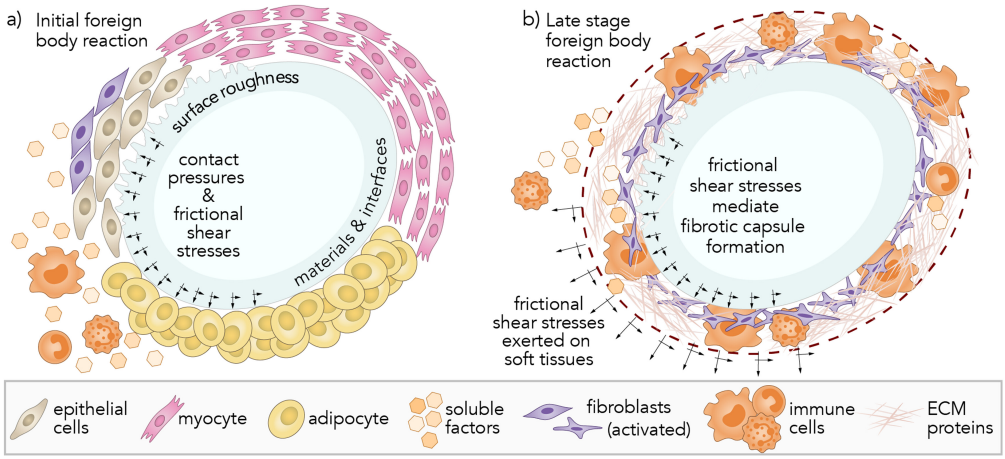

Figure 1. (a) Immediately post-implantation (0–2 weeks), silicone prostheses directly contact and slide against soft tissues, including epithelial cells, myocytes, adipocytes, and extracellular matrix (ECM) proteins, including collagen. The resulting contact pressures and shear stresses across mechanosensitive surfaces are hypothesized to provoke the immune response and initiate the wound healing process. (b) About 2 weeks post-implantation, frictional shear stresses likely mediate the formation of a fibrotic capsule composed of activated fibroblasts, immune cells, and ECM proteins.

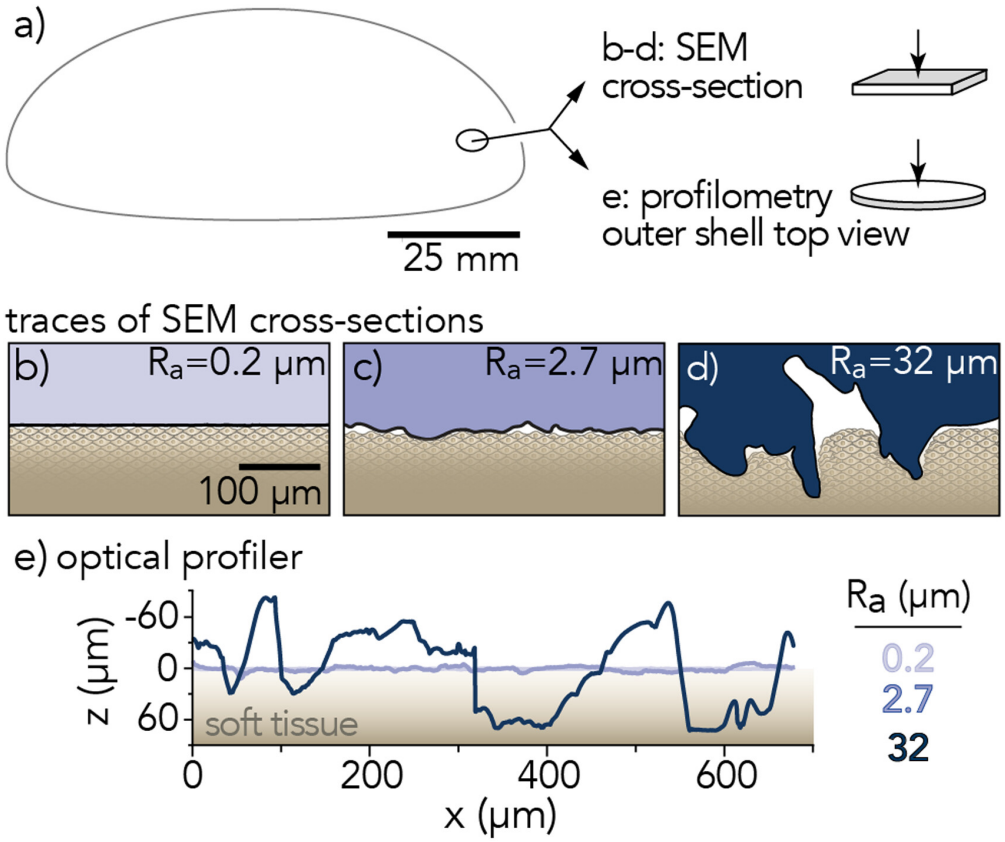

Figure 2. (a) Sections of outer shell removed from breast implant base and prepared for scanning electron microscopy (SEM) and optical surface profilometry. Representative traces of implant surface profiles measured by (b-d) scanning electron microscopy and (e) 3D laser scanning microscopy. Average surface roughness, $\mathbf{R_a}$, was measured from a minimum of 20 line scans across each breast implant shell by surface profilometry: $\mathbf{R_a = 0.2\,\mu m}$ (light purple); $\mathbf{R_a = 2.7\,\mu m}$ (purple); $\mathbf{R_a = 32\,\mu m}$ (dark purple). Line scans were rotated $\mathbf{180^\circ}$ from their original orientation to illustrate how the most prominent surface features may contact and protrude into hypothetical cell layers (drawn to scale) and soft tissues *in vivo*.

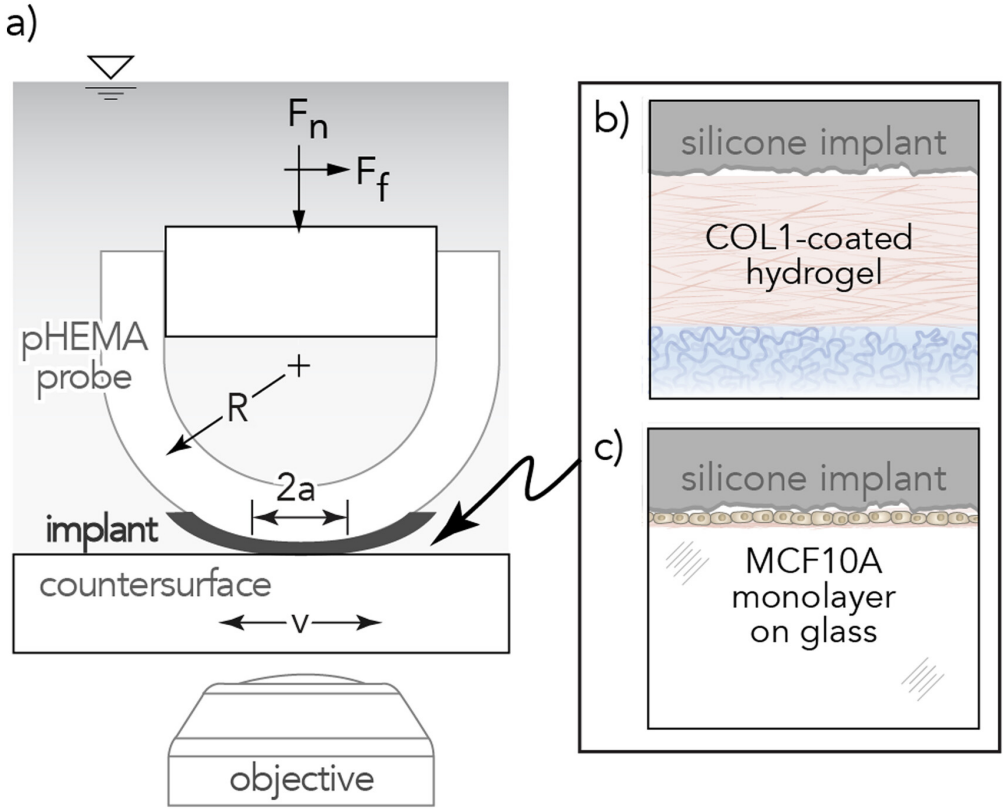

Figure 3. (a) Illustration of biotribometer configuration. Insets of contact between silicone implant and experimental countersurfaces (b) Collagen Type 1, COL1-coated hydrogel and (c) healthy breast epithelia, MCF10A monolayer.

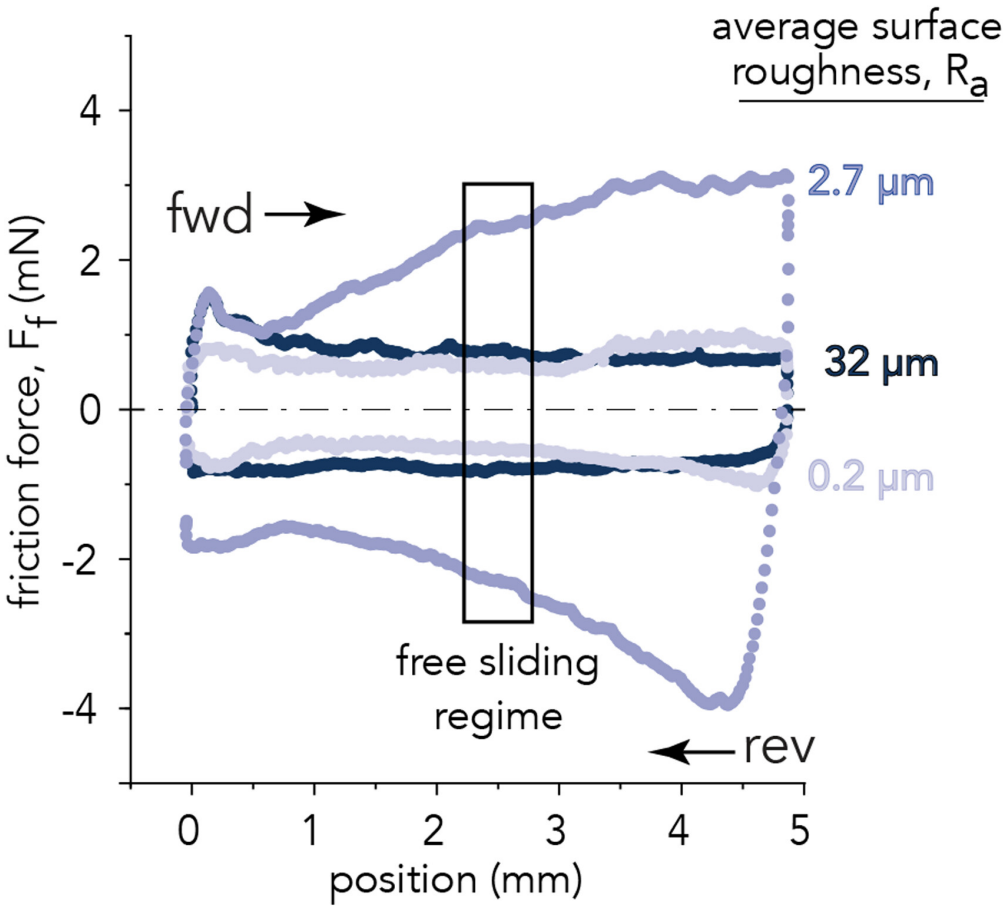

Figure 4. Friction force trace of first reciprocating cycle for three breast implant samples of $\mathbf{R_a = 0.2\,\mu}$m (light purple); $\mathbf{2.7\,\mu}$m (purple); $\mathbf{32\,\mu}$m (dark purple) sliding against COL1-coated polyacrylamide disks submerged in PBS. Experimental conditions: normal load, $F_n = 1.5$ mN; sliding speed, $v = 0.5$ mm/s; sliding path length, $l = 5$ mm (1/2 cycle). Average friction forces and average friction coefficients per cycle were averaged across the middle 10% of the sliding path, within the free sliding regime (n > 50 datapoints).

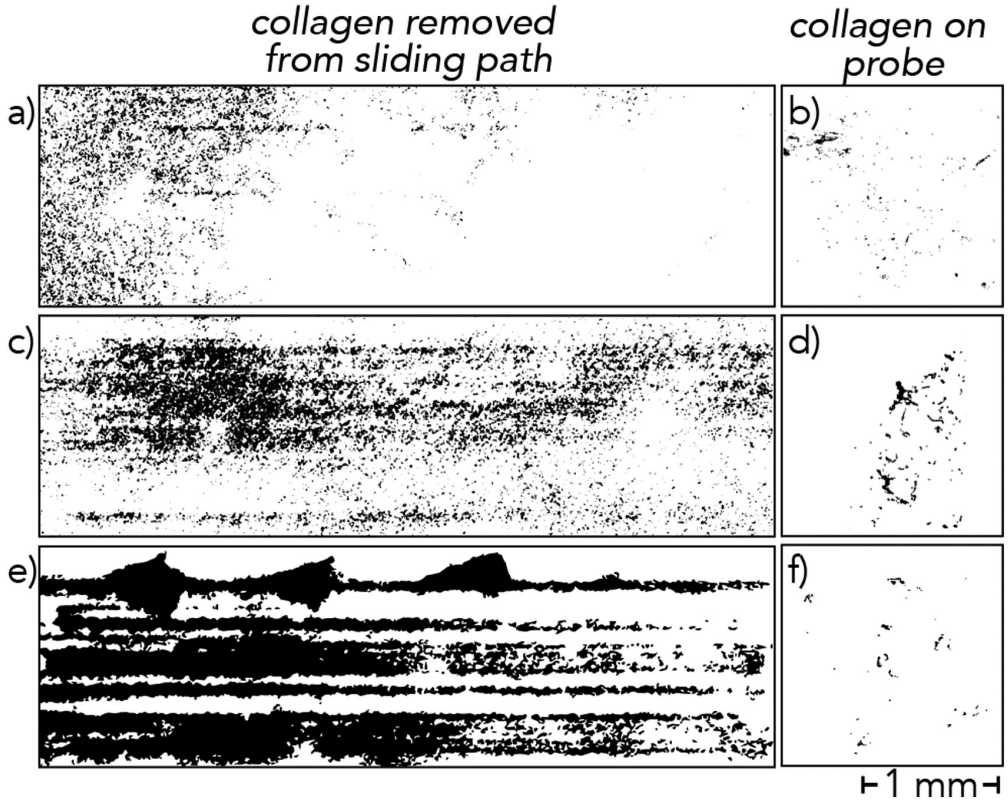

Figure 5. (a,c,e) Collagen removed from polyacrylamide hydrogel substrates and (b,d,f) transferred to the breast implant probe after 1,000 mm total sliding distance. (a,b) $\mathbf{R_a = 0.2\,\mu}$m; (c,d) $\mathbf{R_a = 2.7\,\mu m}$; (e,f) $\mathbf{R_a = 32\,\mu m}$. Increasing average surface roughness increased the total surface area of collagen removed (black) but did not significantly increase amount of collagen adhered (black) to the silicone breast implant at the end of the experiment.

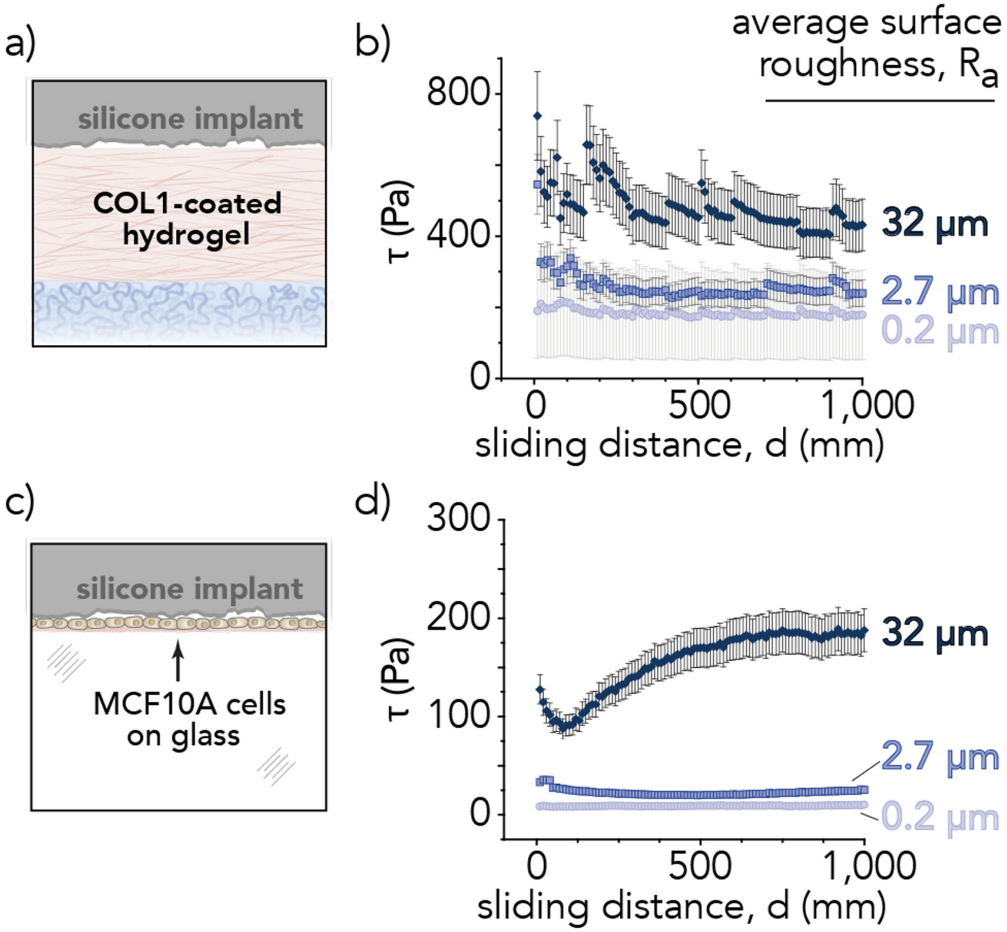

Figure 6. Frictional shear stress as a function of sliding distance for the silicone elastomer implant surfaces ($\mathbf{R_a = 0.2, 2.7, 32\ \mu m}$) against (a,b) COL1-coated hydrogels (n = 2,3,3) and (c,d) MCF10A monolayers (n = 3). (b,d) Frictional shear stress over the entire sliding distance. The "microtextured" implant ($\mathbf{R_a = 32\ \mu m}$) (dark purple) exhibited the highest shear stress across all configurations and sliding distances, while the "smooth" implant with the lowest $\mathbf{R_a}$ ($\mathbf{R_a = 0.2\ \mu m}$) (light purple) exhibited the lowest. Error bars represent the standard deviation in the calculated shear stress across three independent experiments unless otherwise stated.

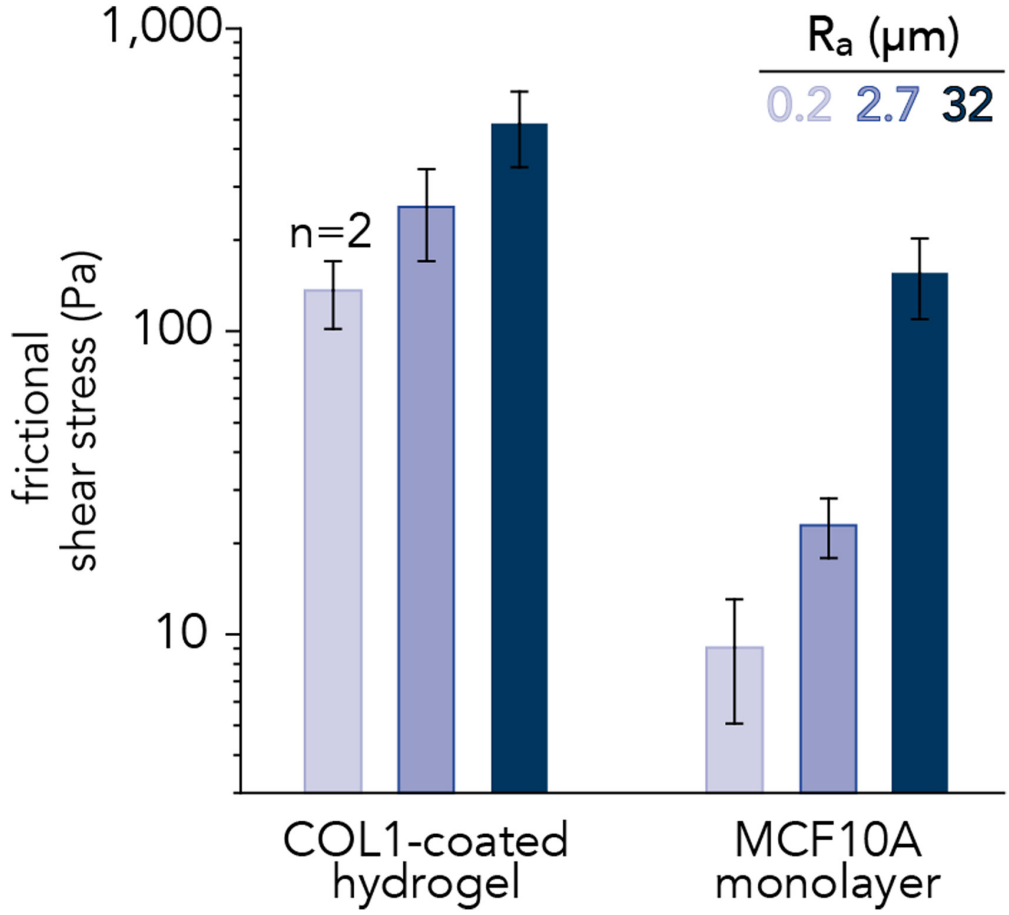

Figure 7. Frictional shear stresses across the sliding interface between silicone implants and model countersurfaces: collagen-coated (COL1) polyacrylamide hydrogels and MCF10A breast epithelial cell monolayers. Shear stress increases with the average surface roughness of breast implant materials ($\mathbf{R_a = 0.2\ \mu m}$, light purple; 2.7 μm, purple; 32 μm, dark purple). Frictional shear stresses below 100 Pa did not result in any visible damage to cell monolayers. Error bars represent standard deviations between experiments (n = 3 for all test unless otherwise stated).

Materials and methods

Implant surface characterization

The surface topography of soft silicone breast implants was evaluated to investigate the role of surface roughness on soft tissue damage *in vitro*. Sections of unused and de-gelled commercially-available silicone breast implant shells were removed near the base (Figure 2(a)) for all analyses, where the contact pressures and frictional shear stresses are greatest against the body.

Thin strips (2 mm wide, 6 mm length) of implant shells were cut with a sharp blade and imaged in cross-section using scanning electron microscopy (SEM) to acquire high-resolution micrographs of the implant surface topography that would be in direct sliding contact with soft tissues (Figure 2(b) to (d) and **Supplementary Materials, Figure S1**). Schematic representations of implant profiles based on SEM micrographs are illustrated in contact with a theoretical tissue roughly drawn to scale in Figure 2(b) to (d). Large sections (6 mm diameter) of breast implant shells were examined using non-contacting 3D laser confocal scanning microscopy (Keyence VK-X3000) (Figure 2(e)). Surface profiles were analyzed over a $700 \times 500\,\mu$m region with at least 20 line scans. The average surface roughness, $\mathbf{R_a}$, of the silicone breast implants in this study spanned three orders of magnitude: Allergan Smooth (

$\mathbf{R} = 0.2 \pm 0.03\,\mu$m), Motiva Ergonomix ($\mathbf{R_a} = 2.7 \pm 0.6\,\mu$m), and Mentor Siltex ($\mathbf{R_a} = 32 \pm 7.0\,\mu$m). The ISO 14607:2018 considers the first two "smooth" ($\mathbf{R_a} < 10\,\mu$m) and the latter "microtextured" ($10\ \mu\mathbf{m} < \mathbf{R_a} < 50\,\mu\mathbf{m}$).[11] These results lie within ranges reported by other researchers.[27–29] Henceforth we will refer to each breast implant surface by its average surface roughness value, $\mathbf{R_a}$. Additional surface roughness parameters for each implant sample are compiled in the **Supplementary Materials (Table S1-4)**. While optical profilometry offers the advantage of high-throughput automated surface analyses, it cannot detect folded or curled features from top-down imaging alone, as in the case of the "microtextured" breast implant surface (Figure 2(d) and (e)).

Soft tissue model surface preparation

To investigate initial damage to the breast pocket following surgical implantation of silicone elastomer implants, we developed simplified *in vitro* models of the implant-tissue sliding interface that incorporated non-cellular (e.g., ECM) and cellular components.[30,31] We conducted tribological measurements (Figure 3(a)) of implants sliding against collagen-coated hydrogels (Figure 3(b)) and healthy breast epithelial cell monolayers (Figure 3(c)).

Collagen-coated hydrogels were composed of polyacrylamide (PAAm) which is a common system used for biological experimentation and protein functionalization.[30] Hydrogel disks (2 mm thickness, 18 mm diameter) were prepared by combining 17.5 wt.% acrylamide, 0.7 wt.% N,N'-methylenebisacrylamide (MBAm), 0.15 wt.% tetramethylenediamine (TEMED), and 0.15 wt.% ammonium persulfate (APS) in ultrapure water (18.2 MΩ). The average elastic modulus of the PAAm hydrogels was approximately 300 kPa (**Supplementary Material, Figure S2.1**), which is the same order of magnitude as soft tissues of the breast pocket, including muscle and skin.[32] Hydrogels were cast between two parallel polystyrene plates and first equilibrated in ultrapure water for at least 24 h and then equilibrated in a zwitterionic sulfonic acid buffering agent, 4 (2-hydroxyethyl)-1-piperazineethanesulfonic acid (HEPES, Gibco, Thermo Fisher Scientific) for at least 24 h prior to functionalization (**Supplementary Materials, Section 3**). Briefly, polyacrylamide disks were immersed in a solution of sulfosuccinimidyl 6-(4'-azido-2'-nitrophenylamino)hexanoate) (sulfo-SANPAH)[30] to anchor collagen layers (Rat Tail Collagen Type I, Corning 354236, $150\ \mu\mathbf{m}$ thickness) and were equilibrated in phosphate-buffered saline (PBS, 1X) for at least 24 h prior to testing.

Healthy breast epithelia (MCF10A, ATCC CRL-10317^{TM}) (Figure 3(c)) were used to model the cellular component of breast pockets. Cell monolayers were cultured in basal mammary growth media (MEBM^{TM} Basal Medium, Lonza CC-3150), plated on fibronectin-coated glass-bottomed culture dishes (20 mm well diameter, #0 cover glass, Cellvis D35200N), and grown to 80% confluence prior to tribological measurements. Quasi-static indentation experiments (normal load, F_n = 1.5 mN; loading velocity, $v = 10\,\mu$m/s) showed no significant adhesion between cell monolayers and implant surfaces over 100 indentation cycles (**Supplementary Materials, Figure S2.2**). All cells used for these studies were between passages 6 and 13.

Implant probe preparation and assembly

Sections of silicone breast implant shells (3 mm radius, 0.5 mm thickness) were mounted with cyanoacrylate adhesive on hydrogel probes with spherical shell geometries such that the exterior implant surface would be exposed.[33] Poly(hydroxyethyl)methacrylate (PHEMA) probes (6 mm radius of curvature, $300\,\mu\mathrm{m}$ apical thickness) were prepared by combining 67 wt.% 2-hydroxyethyl methacrylate (HEMA), 0.2 wt.% MBAm, 0.15 wt.% TEMED, 0.15 wt.% APS, and ultrapure water. Gels were cast within custom polyoxymethylene molds, heated to 60°C for 1 h, and then equilibrated in ultrapure water for at least 24 h. Implant sections were rinsed in PBS and mounted to the apex of the hydrogel probe prior to testing (Figure 3(a)).

In situ Biotribometer

Tribological testing was conducted using a custom linear reciprocating biotribometer mounted to the condenser turret of an inverted laser scanning confocal microscope (Nikon A1R HD). The probe was fastened to a titanium double-leaf cantilever assembly with normal and tangential stiffness of $K_n = 225\,\mu\mathrm{N}/\mu\mathrm{m}$ and $K_t = 122\,\mu\mathrm{N}/\mu\mathrm{m}$, respectively. Capacitance sensors (Lion Precision, sensitivity: $5\,\mu$m/V, range: 20 V) measured cantilever displacements in the normal and tangential directions, correspondingly converted to normal and friction forces. The measurement uncertainties in normal force and friction force were u(F_n) $= \pm 2\,\mu$N and u(F_f) $= \pm 1\,\mu$N, respectively. Composite images of the sliding path (length, $l = 5$ mm; $\frac{1}{2}$ cycle) were collected using the confocal microscope prior to testing and after every 1 sliding cycle through 10, and every 10 cycles until 100; each sliding cycle was a total of 10 mm in length. Implant motions within the breast pocket during the early post-operative period is considered normal; indeed, breast massage and implant displacement techniques are commonly recommended to prevent capsular contracture despite a lack of supporting evidence.[34] Ultrasound images of breast implants have revealed rotations in excess of 30 degrees from original placement, which would lead to 30 mm of sliding distance at the periphery.[35] In this study, the linear reciprocating distance of 10 mm was thus chosen to represent early post-operative implant-tissue sliding distances per day. We assume that the total sliding distance of 1,000 mm is a reasonable approximation of implant motions within the first three months post-implantation.

For each sliding cycle, friction coefficients (μ_{cycle}) were calculated by dividing the average friction force (over the forward, $F_{f_{fwd}}$, and reverse, $F_{f_{rev}}$, directions) by the average normal force (F_n) within the free sliding regime (middle 10% of the sliding path, n > 50) (Equation 1). For more details, see **Supplementary Materials, Section 4**.

$$\mu_{cycle} = \frac{\left\langle F_{f_{fwd}} \right\rangle - \left\langle F_{f_{rev}} \right\rangle}{2\left\langle F_n \right\rangle} \tag{1}$$

Silicone breast implant probes were loaded against COL1-coated polyacrylamide disks and MCF10A-coated coverslips to $F_n = 1.5$ mN and sliding was conducted at a constant velocity of $v = 0.5$ mm/s. Probes and disks were fully submerged for the duration of testing, and new tribological pairs were used for each experiment. Tribological experiments with COL1-coated disks were conducted under ambient

conditions (20° C and in PBS). Tribological experiments using MCF10A monolayers were conducted in basal mammary growth medium and at physiological conditions using a custom built incubator chamber (37°C, 5% CO_2, >95% RH).

Results and discussion

Tribological measurements

Surface roughness has long been known to influence the tribological properties of elastic bodies in sliding contact and the relationship is strongly dependent on material,[36] environmental,[37] and testing conditions.[38–40] For breast implant materials in sliding contact with COL1-coated hydrogels, the outer shell's surface roughness did not correlate with friction force (Figure 4). Image analyses of the sliding path revealed that increased surface roughness led to greater removal of collagen from the hydrogel substrate (Figure 5(a,c,e)). Analysis of the wear track over time and sliding distance demonstrated increasing collagen removal at constant normal force **(Supplementary Figure S3)**. The amount of collagen transferred from the hydrogel surface to the implant-covered probe did not appear to follow this same trend; all three probes revealed at least some collagen transfer regardless of surface roughness (Figure 5(b,d,f)). Collagen transfer was exclusively based on qualitative fluorescence measurements and thus it is difficult to draw quantitative conclusions regarding the total amount of collagen that may have transferred to probes over the course of the study as opposed to lost in solution. Another limitation is that breast implant-covered probes were only imaged before and after sliding experiments. Images of collagen removal (Figure 5(a,c,e), **Supplementary Videos 1-3**) were used to determine the apparent area of contact during sliding, which decreased with increasing surface roughness (from low to high $\mathrm{R_a}$, $A_{apparent} \approx 2.11\,\mathrm{mm^2}, 1.5\,\mathrm{mm^2}$, and 0.87 $\mathrm{mm^2}$, respectively) under the same normal loads. These results contrasted with the expected contact area of smooth ($\mathrm{R_a} < 100$ nm) spherically-capped shell probes, which increases in proportion with normal load, resulting in constant contact pressure. Trends of apparent contact area from dynamic sliding measurements agreed with static contact area measurements and observations of collagen transferred to probes at the end of sliding experiments (Figure 5(b,d,f)). The apparent area of contact was used to estimate the frictional shear stresses, τ, reacting across the sliding interface using Equation 2, where μ_{avg} is the average friction coefficient and $F_{n_{avg}}$ is the average normal force over the observation period.

$$\tau = \mu_{avg}\left(\frac{F_{n_{avg}}}{A_{apparent}}\right) \tag{2}$$

Frictional shear stress measurements over sliding distance provide further context for *in vitro* soft tissue trauma (Figure 6). Frictional shear stress between implants and COL1-coated polyacrylamide countersurfaces generally decreased over sliding distance, which correlated with collagen removal. Uncoated polyacrylamide control countersurfaces confirmed that the greatest source of frictional shear stresses was the collagen coating (**Supplemental Material, Figure S4**). Increasing average surface roughness likely increases frictional shear stresses and may induce damage to soft tissues, as shown in

the simplified *in vitro* model herein. Unlike the “smooth” breast implant materials, which distribute the normal force over a larger surface area and reduce frictional shear stresses, the relatively high surface roughness of the “microtextured” breast implant surface effectively concentrates all normal and friction forces over a smaller number of surface asperities and a reduced apparent contact area, which results in increased contact pressure. During sliding, contact pressures from prominent asperities likely increase frictional shear stresses even if the average friction coefficient remains constant. Previous investigations using epithelial cell monolayers have shown that frictional shear stresses in excess of $\tau = 40$ Pa are sufficient to upregulate pro-inflammatory gene expression[41,42] and can lead to cell rupture beyond $\tau = 100$ Pa.[43] Frictional shear stresses measured for all three breast implants sliding against COL1-coated gels (Figure 7) exceeded 100 Pa yet resulted in varying damage to collagen surface layers. Average frictional shear stress measurements within groups (similar countersurface, different $\mathbf{R_a}$ values) showed significant differences ($p < 0.05$), and average frictional shear stress measurements across groups (different countersurfaces, same $\mathbf{R_a}$ value) showed significant differences ($p < 0.05$) by Student’s t-test. These results indicate collagen is not an inherently low friction extracellular matrix protein, which may provide a route to understanding chronic inflammation due to fibrosis or the mechanisms of adverse cellular remodeling during wound healing or in response to foreign bodies.[44,45]

To investigate soft tissue damage *in vitro* with a simple cellular model of the breast pocket, human breast epithelial (MCF10A) cell monolayers were subjected to identical tribological challenges (with the exception of growth media in place of PBS). Cells were stained using a fluorescent propidium iodide (PI) live/dead assay to clearly identify dead cells (**Supplementary Materials, Figure S5**). For breast implants with the two lowest surface roughness, $\mathbf{R_a} = 0.2\,\mu\mathrm{m}$ and 2.7 μm, MCF10A cells remained alive and retained normal cellular morphology. In fact, cells within and outside of the sliding path were indistinguishable in brightfield and phase-contrast imaging (Nikon Ti2 widefield microscope). These results are unsurprising in light of the estimated frictional shear stresses, which were below $\tau = 100$ Pa for both of these breast implants ($\mathbf{R_a} = 0.2\,\mu\mathrm{m}$ and $2.7\,\mu\mathrm{m}$). In contrast, the breast implant material with highest surface roughness ($\mathbf{R_a} = 32\,\mu\mathrm{m}$) resulted in frictional shear stresses in excess of $\tau = 100$ Pa and left ploughed-like regions of monolayer delamination ringed by red fluorescent dead cells, which correspond well with the length-scales of the most prominent surface features (**Supplementary Materials, Figure S5**).

Frictional shear stress measurements demonstrate the utility of these *in vitro* soft tissue models and enabled our investigation into COL1- and MCF10A-implant interfaces. These biological interfaces present unmet tribological design challenges for implant materials. These studies are limited by the fact that cell monolayers were plated on fibronectin-coated glass and not on COL1-coated hydrogel substrates. Another limitation is that the sliding experiments were conducted over the span of a few hours, which may be insufficient to observe substantive cellular remodeling or morphological changes. Future investigations will extend this work to provide deeper analysis of cell responses to repeated mechanical microtraumas.

Conclusions

In this investigation, we developed an *in vitro* method to systematically characterize silicone breast implant surface roughness induced soft tissue damage on COL1-coated polyacrylamide hydrogel surfaces and MCF10A cell monolayers. Our findings suggest that “smooth” silicone elastomer breast implants ($\mathbf{R_a} < 10\,\mu\mathbf{m}$) result in lower frictional shear stresses, moderate COL1 removal, and no visible damage to cell monolayers. In contrast, “microtextured” silicone elastomer breast implants ($10\,\mu\mathbf{m} < \mathbf{R_a} < 50\,\mu\mathbf{m}$) result in higher frictional shear stresses, extensive COL1 removal, and significant cell death as indicated by propidium iodide staining. These findings highlight the importance of designing soft breast implants with low surface roughness to reduce frictional shear stresses and avoid adverse physiological responses.

Acknowledgements

This manuscript is dedicated to the memory of Duncan and Mabel Dowson, whose generosity of spirit is a continual source of inspiration. We are grateful to Kylie E. Van Meter for helpful discussions on early designs of the probe assembly. We are grateful for helpful discussions with Dr. Juan Manuel Urueña.

Declaration of conflicting interests

The authors declared no potential conflicts of interest with respect to the research, authorship, and/or publication of this article.

Funding

This work was partially supported by the National Science Foundation (NSF) Materials Research Science and Engineering Center (MRSEC) at UC Santa Barbara through DMR-1720256 (IRG-3). The use of the shared facilities of the MRSEC is gratefully acknowledged; the UCSB MRSEC is a member of the Materials Research Facilities Network (www.mrfn.org). This work was partially supported by the BioPACIFIC Materials Innovation Platform of the National Science Foundation under Award No. DMR-1933487. This work was partially supported by Establishment Labs, Costa Rica. Establishment Labs did not take part in the study design, collection or analysis of the data; in writing the journal article, or the decision to submit for publication. J.M.R. acknowledges support from the Gates Millennium Scholarship through the Bill and Melinda Gates Foundation and Hispanic Scholarship Fund. A.L.C. acknowledges support of the National Science Foundation Graduate Research Fellowship Program under Grant No. 1650114. R.B. acknowledges support from the Future Leaders in Advanced Materials (FLAM) program (DMR-1720256). R.I.E.L. acknowledges support from the University of California Leadership Excellence through Advanced Degrees (UC LEADS) program. A.A.P. acknowledges funding support from the NSF CAREER award (CMMI-CAREER-2048043).

ORCID iD

Angela A. Pitenis https://orcid.org/0000-0002-9697-7291

Notes

Data accessibility	The data that support the findings of this study are available from the corresponding author, upon reasonable request.
Supplemental material	Supplemental material for this article is available online.

References

1. Curtis J, Steichen SD. 1.3.2b – Silicones. In: Wagner WR, Sakiyama-Elbert SE, Zhang G, and Yaszemski MJ (eds) *Biomaterials Science (Fourth Edition)*. Cambridge: Academic Press, 2020, pp.109–123.
2. Hallab NJ, Samelko L, Hammond D. The inflammatory effects of breast implant particulate shedding: Comparison with orthopedic implants. *Aesthet Surg J* 2019; 39: S36–S48.
3. Headon H, Kasem A, Mokbel K. Capsular contracture after breast augmentation: An update for clinical practice. *Arch Plast Surg* 2015; 42: 532–543.
4. Manikkam Umakanthan J, McBride CL, Greiner T, et al. Bariatric implant-associated anaplastic large-cell lymphoma. *J Oncol Pract* 2017; 13: 838–839.
5. DeCoster RC, Clemens MW, Di Napoli A, et al. Cellular and molecular mechanisms of breast implant–associated anaplastic large cell lymphoma. *Plast Reconstr Surg* 2021; 147: p 30e–41e.
6. Doren EL, Miranda RN, Selber JC, et al. U.S. epidemiology of breast implant–associated anaplastic large cell lymphoma. *Plast Reconstr Surg* 2017; 139: 1042–1050.
7. Shauly O, Gould DJ, Siddiqi I, et al. The first reported case of gluteal implant-associated anaplastic large cell lymphoma (ALCL). *Aesthet Surg J* 2019; 39: NP253–NP258.
8. Williams DF. There is no such thing as a biocompatible material. *Biomaterials* 2014; 35: 10009–10014.
9. Black J, Black J. Biological performance of materials: Fundamentals of biocompatibility. Boca Raton, FL: CRC Press, 2005.
10. Black J. Systemic effects of biomaterials. In: Williams D (ed) *The Biomaterials: Silver Jubilee Compendium*. Oxford: Elsevier Science, 1984, pp.27–34.
11. ISO14607:2018: Non-active surgical implants — Mammary implants — Particular requirements. 2018.
12. Swanson E. Plastic surgeons defend textured breast implants at 2019 U.S. Food and drug administration hearing: Why it is time to reconsider. *Plast Reconstr Surg Glob Open* 2019; 7: e2410.
13. Dowson D. Bio-tribology. *Faraday Discuss* 2012; 156: 9–30.
14. ISO10993-1: Biological Evaluation of Medical Devices - Part 1: Evaluation and Testing Within a Risk Management Process. 2018.
15. Noskovicova N, Hinz B, Pakshir P. Implant fibrosis and the underappreciated role of myofibroblasts in the foreign body reaction. *Cells* 2021; 10: 1794.
16. Anderson JM, Rodriguez A, Chang DT. Foreign body reaction to biomaterials. *Semin Immunol* 2008; 20: 86–100. Innate and Adaptive Immune Responses in Tissue Engineering.
17. Anderson JM. Exploiting the inflammatory response on biomaterials research and development. *J Mater Sci Mater Med* 2015; 26: 121.
18. Witherel CE, Abebayehu D, Barker TH, et al. Macrophage and fibroblast interactions in biomaterial-mediated fibrosis. *Adv Healthc Mater* 2019; 8: 1801451.
19. Tolman DE, Laney WR. Tissue-integrated prosthesis complications. *Int J Oral Maxillofac Implants* 1992; 7: 477–484.
20. Deva AK, Adams WPJ, Vickery K. The role of bacterial biofilms in device-associated infection. *Plast Reconstr Surg* 2013; 132: 1319–1328.
21. Deva AK, Adams WPJ, Vickery K. The role of bacterial biofilms in device-associated infection. *Plast Reconstr Surg* 2013; 132: 1319–1328.

22. Coroneos CJ, Selber JC, Offodile ACI, et al. Us fda breast implant postapproval studies: Long-term outcomes in 99, 993 patients. *Ann Surg* 2019; 269: 30–36.

23. Pitenis AA, Urueña JM, McGhee EO, et al. Challenges and opportunities in soft tribology. *Tribol - Mater, Surface Interface* 2017; 11: 180–186.

24. Urueña JM, Hart SM, Hood DL, et al. Considerations for biotribometers: Cells, gels, and tissues. *Tribol Lett* 2018; 66: 141.

25. Cobb JA, Dunn AC, Kwan J, et al. A Novel Method for Frictional Testing on Adherent Cells. *Proceedings of the ASME 2007 Summer Bioengineering Conference*. *ASME 2007 Summer Bioengineering Conference*. Keystone, Colorado: ASME, 2007, pp. 821–822.

26. Clark ER, Hemmings K, Greco S, et al. Tribological characteristics of human vascular smooth muscle cells: The implication of disease state on friction. *Biotribology* 2020; 22: 100122.

27. Nava MB, Catanuto G, De Vita R, et al. Comment on: Breast implant surfaces and their impact on current practices: Where are we now and where are we going. *Plast Reconstr Surg Glob Open* 2020; 8: e2639.

28. Doloff JC, Veiseh O, de Mezerville R, et al. The surface topography of silicone breast implants mediates the foreign body response in mice, rabbits and humans. *Nat Biomed Eng* 2021; 5: 1–16.

29. Pitenis AA, Sawyer WG. Soft textured implants: Roughness, friction, and the complications. *Biotribology* 2020; 22: 100127.

30. Chaudhuri T, Rehfeldt F, Sweeney HL, et al. *Preparation of Collagen-Coated Gels that Maximize In Vitro Myogenesis of Stem Cells by Matching the Lateral Elasticity of In Vivo Muscle*. Totowa, NJ: Humana Press, 2010, pp.185–202.

31. Kim C-L, Kim D-E. Self-healing characteristics of collagen coatings with respect to surface abrasion. *Sci Rep* 2016; 6: 20563–20563.

32. Gefen A, Dilmoney B. Mechanics of the normal woman's breast. *Technol Health Care: Off J Eur Soc Eng Med* 2007; 15: 259–271.

33. Marshall SL, Schulze KD, Hart SM, et al. Spherically capped membrane probes for low contact pressure tribology. *Biotribology* 2017; 11: 69–72.

34. Sood A, Xue EY, Sangiovanni C, et al. Breast massage, implant displacement, and prevention of capsular contracture after breast augmentation with implants: A review of the literature. *Eplasty* 2017; 17: e41.

35. Sieber DA, Stark RY, Chase S, et al. Clinical evaluation of shaped gel breast implant rotation using high-resolution ultrasound. *Aesthet Surg J* 2017; 37: 290–296.

36. Persson BNJ, Albohr O, Tartaglino U, et al. On the nature of surface roughness with application to contact mechanics, sealing, rubber friction and adhesion. *J Phys, Condens Matter* 2004; 17: R1–R62.

37. Bowden FP and Tabor D. Frank Philip, *The friction and lubrication of solids*. Oxford University Press, 1950.

38. Wu-Bavouzet F, Cayer-Barrioz J, Le Bot A, et al. Effect of surface pattern on the adhesive friction of elastomers. *Phys Rev E* 2010; 82: 031806.

39. Degrandi-Contraires E, Poulard C, Restagno F, et al. Sliding friction at soft micropatterned elastomer interfaces. *Faraday Discuss* 2012; 156: 255–265.

40. Denny DF. The influence of load and surface roughness on the friction of rubber-like materials. *Proc Phys Soc Sec B* sep 1953; 66: 721–727.

41. Pitenis AA, Urueña JM, Hart SM, et al. Friction-induced inflammation. *Tribol Lett* 2018; 66: 81.

42. Chau AL, Rosas J, Degen GD, et al. Aqueous surface gels as low friction interfaces to mitigate implant-associated inflammation. *J Mater Chem B* 2020; 8: 6782–6791.
43. Hart SM, Degen GD, Urueña JM, et al. Friction-induced apoptosis. *Tribol Lett* 2019; 67: 82.
44. Rodrigues M, Kosaric N, Bonham CA, et al. Wound healing: A cellular perspective. *Physiol Rev* 2019; 99: 665–706.
45. Anderson JM, Rodriguez A, Chang DT. Foreign body reaction to biomaterials. *Semin Immunol* 2008; 20: 86–100.